A Comparative Study of Spark Plasma and Conventional Sintering of Undoped SnO_2 Sputtering Targets

Levent Koroglu
Eskişehir Technical University: Eskisehir Teknik Universitesi
Cem Aciksari
Eskişehir Technical University: Eskisehir Teknik Universitesi
Erhan Ayas (erayas@eskisehir.edu.tr)
Eskişehir Technical University: Eskisehir Teknik Universitesi
Emel Ozel
Eskişehir Technical University: Eskisehir Teknik Universitesi
Ender Suvaci
Eskişehir Technical University: Eskisehir Teknik Universitesi

Research Article

Keywords: SnO2, Spark Plasma Sintering, Conventional Sintering, Undoped, Sputtering Targets

Posted Date: June 24th, 2021

DOI: https://doi.org/10.21203/rs.3.rs-646052/v1

Abstract

SnO_2 ceramics were fabricated by spark plasma sintering (SPS) and conventional (pressureless) sintering techniques by using undoped submicron SnO_2 powders. The effect of sintering temperature and dwell time on the densification behavior, phase evolution and microstructural development of sintered ceramics were investigated. The relative density of SPSed ceramics increased when dwell time was raised from 1 to 10 min at 950ºC. However, full densification was prevented by the decomposition of SnO_2 to Sn and O_2(g). The decomposition starts after ~ 10 min at 950ºC. In parallel to this observations, as sintering temperature increases, amount of the elemental Sn in agglomerated form increases. On the other hand, the relative densities of conventionally sintered ceramics (at 1200ºC-1400ºC) were relatively low (i.e., 63 % relative density), and abnormal grain growth was observed due to the shift in sintering mechanisms to evaporation-condensation as a dominant mechanism. Since the undoped SnO_2 ceramics, SPSed at 950°C for 5 min under 30 MPa exhibit 93 % relative density, high chemical purity, homogeneous grain size distribution and smaller average grain size, they demonstrate great potential as sputtering targets for production of high-quality thin film gas sensors.

1 Introduction

Tin oxide (SnO_2) is a critical electronic material which has been widely used in an extensive range of applications such as gas sensor [1], varistor in electronic devices [2], electro/photocatalyst [3, 4], transparent conductive oxide films [5] and optoelectronic devices [6]. The most important application field of SnO_2 material is in metal oxide semiconductor (MOS) based gas sensors. The MOS sensors are the most preferred and currently used devices among the other sensing mechanisms such as catalytic, electrochemical, and NDIR (Non-Dispersive Infrared) types to detect the pollutant gases (CO, CO_2, NO_x, SO_x, $VOC_{s,}$ etc.) results in diminishing the air quality.

SnO_2 based materials can be deposited into the gas sensing devices in the form of thick or thin films [7]. Thick films are composed of porous SnO_2 in a thickness of 1 to 10 microns produced from the slurry form. Thin films, on the other hand, have a thickness of 10 nm to 1 micron. Several methods were used to prepare SnO_2 based gas sensors, such as thermal evaporation [8], dip and spin coating [9], and hydro/solvothermal method [10, 11]. For industrial aspects, sputtering is a widely accepted route for preparing SnO_2 thin films used in gas sensing applications among these methods. Sputtering process can be performed from either metallic or ceramic targets. Ceramic targets are preferred to produce thin films with higher quality and reproductively. They have homogeneous optical and electrical properties along with the material, whereas the metallic one is cheaper and more accessible in the market and has higher thermal conductivity. One of the well-known problems during sputtering is the formation of nodules on the target material [12, 13]. The nodules formed by the arching during the sputtering can result in the uncontrolled highly defective film. The arching is mainly related to the non-homogeneity in the chemical, physical, microstructural, and electrical properties of the sputter target. In addition to that, inhomogeneous grain size, a minimum amount of pores and higher density prevent the formation of

nodules. The formation of particles during the sputtering process is one of the significant problems which originate from nodules on the target surface. To overcome the nodule and related causes during the sputtering process, target material should be manufactured with higher density (> 92 % of SnO_2 relative density), higher chemical purity (> 99.95 wt.% of SnO_2), homogeneous distribution of cations and oxygen mainly in the surface and higher thermal and mechanical stability to reduce the chance of target cracking. Even ceramics with a density of greater than 98% of its relative density and high electrical conductivity are strongly required for DC magnetron sputtering systems employed in the industry [14].

It is crucial to produce dense SnO_2 sputtering targets with homogenous grain size distribution and high chemical purity which provides low electrical resistivity and high thermal and mechanical stability due to getting relatively higher performance in the sputtering process. However, it is difficult to achieve full densification by pressureless-assisted sintering due to the decomposition of SnO_2(s) to SnO(g) above 1200ºC where evaporation-condensation takes place [15]. Therefore, it is concluded with only coarsening of tin oxide ceramics with very low densification (60 % relative density) [14]. Leite et al. [16] investigated pressureless-assisted sintering kinetics of ultrafine undoped SnO_2 powder under atmospheric conditions. The results showed that the decomposition rate of SnO_2 increases above 1300ºC with the decreasing particle size of starting SnO_2 powder (from approximately 100 to 25 nm).

Possible technique to produce tin oxide-based ceramics with a higher density is pressure-assisting sintering [14]. Spark plasma sintering (SPS, FAST) is one of the most favorable sintering techniques in which dense polycrystalline materials are produced in bulk form through powder metallurgy under applied pressure. In comparison with the conventional methods and other sintering techniques such as hot press (HP) and hot isostatic pressing (HIP), SPS is fundamentally different in terms of working principle, which is based on the generation of high pulsed electric current. Thus, both electrical field and joule heating are provided along with uniaxial pressure. This phenomenon comes with some advantages such as; high-speed diffusion, full densification, elimination of impurities on the surface of particles, reduction of sintering temperature, shorting of sintering time, and improving mechanical and electrical properties [17–19].

A few types of research in the literature focus on the pressure-assisted sintering of undoped SnO_2 powders. Yoshinaka et al. [20] achieved 99.8 % relative density by Hot Isostatic Pressing at 900°C for 2 h under 196 MPa using argon gas following by isostatically cold pressing of synthesized undoped SnO_2 powders under 343 MPa. Dense SnO_2 ceramic has 10^3 ohm.cm electrical resistivities and approximately 2.0 μm average grain size, as determined by a linear intercept method. In 2005, Park et al. [21] focused on the spark plasma sintering of undoped SnO_2 powders using commercial undoped SnO_2 powder (60 nm crystallite size), and they investigated the variation of the relative density and the weight loss with the sintering temperature. It is reported that weight loss began to occur above 1050ºC. The sintered ceramic by spark plasma sintering at 1050ºC for 5 min under 37.5 MPa exhibited the maximum relative density (around 95 %). That is the only study in the literature based on the spark plasma sintering of undoped SnO_2 powders. Unfortunately, the decomposition of SnO_2 did not discuss in detail; there was no data

regarding the phase evolution and microstructural development. Park et al. only focused on the microstructure analysis of SnO_2 ceramic sintered at 1050ºC in terms of the formation of pores and the homogeneity of microstructure. Delorme et al. [22] stated that undoped SnO_2 ceramics were produced by SPS in order to improve transport properties that are sensitive to doping elements of oxides (CoO, MnO_2, CuO, ZnO, etc.). In this study, they achieved almost 95 % relative density at 950ºC for 10 min under 100 MPa. Delorme et al. mainly focused on the electrical and thermal conductivity of SnO_2 ceramics, which were obtained at different SPS conditions. However, this study does not reflect detailed microstructural development among thermodynamical approaches to understand densification behaviour of SnO_2 ceramics under SPS conditions. A correlative assessment of chemical purity, density, homogenously distributed grains, and small grain size of sputtering targets is crucial to both investigate and improve the performance of sputtering targets. To eliminate this shortage in the literature, in the present study, it is aimed to develop a fundamental understanding of defining ideal microstructure and its effect on final target properties based on densification behavior, phase evolution, and microstructural development in order to get higher performance and efficiency during the sputtering process and achieve higher quality of as-produced thin films as well. Therefore, in this paper, the effects of process conditions on densification behavior, phase evolution and microstructural development of SnO_2 ceramic sputter targets obtained from undoped submicron commercially available SnO_2 powders were systematically investigated as a function of sintering temperature (850-1050°C) and time (1–10 min), while the particle size of starting powder, external pressure, atmospheric conditions, and heating & cooling rates keep constant. Furthermore, the results obtained from SPSed ceramics were compared to conventionally sintered SnO_2 ceramics and commercial SnO_2 targets.

2 Experimental Procedures

2.1 Characterization of the starting powder

Specific surface area of the commercially available tin (IV) oxide (SnO_2; 99.9 %; Merck KGaA) submicron powder was measured by Brunnauer-Emmett-Teller (BET) surface adsorption method (Quantacrom Autosorb 1C). The sample was degassed at 200°C for 4 h under vacuum conditions prior to the measurement. The average particle size (i.e., equivalent spherical diameter), assuming that the particle is spherical and nonporous, was calculated from the BET surface area via equation ($SS = 6/\rho.D$ where SS is specific surface area of the particles in m^2/g, ρ is theoretical density of the particle and D is the particle size).

The qualitative phase analysis was performed using an x-ray diffractometer (XRD; MiniFlex600, Rigaku). Particle size and distribution were measured using a scanning electron microscope (SEM; Supra 50VP, Zeiss).

Chemical purity of the SnO_2 was determined by x-ray fluorescence (XRF, Rigaku ZSX Primus).

2.2 Sintering of undoped SnO_2 ceramics

Densification of SnO_2 submicron powder without any sintering additive was achieved using spark plasma sintering furnace (HPD-50, FCT GmbH, Germany) under a vacuum atmosphere. The process parameters such as sintering temperature and holding time were optimized to fabricate dense SnO_2 ceramics. During all sintering cycles, heating rate (200ºC/min), cooling rate (switching power off, approximately 600ºC/min), and external pressure (30 MPa) were kept constant. 4 grams of powder were loaded into a graphite die with an inner diameter of 20 mm. Graphite foil was incorporated on the inner surface of graphite die to prevent the reaction between the graphite die and powder. The temperature was increased by the controlled electrical current with the pulse timing of 12:2, and it was monitored by optical pyrometer inside the graphite punches. In order to compare spark plasma sintering with conventional sintering technique, undoped SnO_2 ceramics were also sintered by presureless method (Carbolite Lab Furnace) under conditions (1200ºC, 2 h, 1 atm, 5°C/min) optimized in a prior study [23]. The samples with 50 mm diameter were prepared via uniaxial pressing under 200 MPa for conventional sintering.

Using the submicron starting powder lieS in its high specific surface area and high surface curvature, which improve the sintering rate. Henrring equation explains well the importance of particle size on densification. For instance, when the particle size is 2 times higher, the sintering time is 16 times, where the grain boundary diffusion is dominant [24, 25]. Leite et al. [16] investigated the grain growth kinetics of nanometric undoped SnO_2 powder in the temperature range of 500–1300ºC. Experimental results showed that the mass transport mechanism was controlled by surface diffusion between 500–1000ºC. The thermodynamic driving force for sintering is the reduction in total interfacial energy by diffusion. The differences in bulk pressure, vapor pressure, and vacancy concentration depending on interface curvature yield material transport in terms of kinetics [24]. Different mass transport mechanisms occur during sintering, such as lattice diffusion, grain boundary diffusion, surface diffusion, viscous flow, and gas-phase transport. Some of these sintering mechanisms contribute to densification, whereas others (e.g. surface diffusion) lead to grain growth without densification, which are called non-densifying mechanisms. The dominant densification mechanism depends on experimental and compact conditions such as particle size, neck radius, temperature, time, and pressure [24, 26]. In order to limit the surface diffusion as a non-densifying mechanism, a high heating rate of 200°C/m was constantly applied during spark plasma sintering of SnO_2 ceramics.

2.3 Characterization of the sintered ceramics

After removing the graphite foil layer on the surface of SPSed samples (designated as

SPS-SnO_2), the bulk densities of sintered ceramics were determined by the Archimedes method. In order to calculate the relative density, the density value obtained by Archimedes' principle was divided to 6.95 g/cm^3 (SnO_2 theoretical density). SnO_2 ceramics were crushed and ground under 63 µm. Qualitative phase analysis was performed using XRD (MiniFlex600, Rigaku) with a scan speed of 2°/min at 40 V and

15A. Phase determination was carried out by the Rietveld method using Material Analysis Using Diffraction (MAUD) software. The fractured surface (cross-sectional area) of samples was polished by the automatic polishing machine (TegraPol-25, Struers). Then, all polished samples were thermally etched at a temperature of 200ºC lower than sintering temperature to observe fine microstructure. The microstructure analysis and quantitative elemental analysis carried out using SEM (Supra 50VP, Zeiss). In addition, undoped SnO_2 ceramics fabricated by conventional technique (designated as CS-SnO_2) and a commercial SnO_2 target purchased from a target manufacturer (designated as CM-SnO_2) were also characterized by the same techniques.

3 Results And Discussion

3.1 Characterization of the starting SnO_2 powder

XRD pattern and SEM image of starting powder are illustrated in Fig. 1 and Fig. 2. The powder is composed of only Cassiterite (SnO_2; JCPDS #41-1445), a Rutile type of crystal structure. According to the SEM image of starting powder, the particle size of SnO_2 particles is ranging from 100 to 500 nm with irregular morphologies. The average particle size measured from the SE images is 150 nm. The specific surface area and calculated equivalent spherical diameter of starting powder particle size by the BET method are 7.6 m^2/g and 110 nm, respectively. The chemical purity of the starting SnO_2 powder measured by XRF is shown in Table 1. The SnO_2 powders have high purity and are suitable for the sputtering process without any purification before sintering. The loss on ignition value is neglected due to its shallow value (< 0.1 %).

Table 1
XRF results of pressed SnO_2 starting powder

Elements in oxide	SnO_2	Fe_2O_3	Others (Na_2O, SiO_2, Al_2O_3)
Mass fraction (%)	99.950	0.025	0.025

3.2 Spark plasma sintering of undoped SnO_2

Table 2
Sintering parameters and properties of SnO_2 ceramics sintered by different techniques

Sample Code	Pressure (MPa)	H. Rate (°C/min)	S. Temp. (°C)	D. Time (min)	R. Density (% ±1)	Grain Size (Average in μm)
SPS0-SnO_2	30	200	850	10	70	-
SPS1-SnO_2	30	200	950	1	82	~ 0.5
SPS2-SnO_2	30	200	950	3	87	~ 0.5
SPS3-SnO_2	30	200	950	5	93	~ 0.3
SPS4-SnO_2	30	200	950	10	94	0.2–0.3
SPS5-SnO_2	30	200	1050	10	94	~ 0.5
CS1-SnO_2	0.1	10	1200	120	63	0.5
CS2-SnO_2	0.1	10	1300	120	63	1.0
CS3-SnO_2	0.1	10	1400	120	63	3.0
CM-SnO_2	N. A.	N. A.	N. A.	N. A.	63	3.0–5.0
* N.A.: Not available						

Sintering parameters and properties of sintered ceramics are given in Table 2. For constantly applied pressure, heating rate, sintering temperature (950°C), with the increment of dwell time from 1 to 10 min, relative density of SPSed SnO_2 increased from 82 to 94 %. The relative density values of SPS1-SnO_2 and SPS2-SnO_2 are found below 92 %, which signs the limited densification into the second step. The relative density gradually increases from 82 to 93 % with the increment of dwell time from 1 min to 5 min. When the dwell time increases from 5 min to 10 min, the relative density increases only 2 % (up to 94 %), and average grain size reduces unexpectedly. It is consistent with theoretical knowledge that the required sintering time for densification exponentially increases while the relative density reaches maximum point [24]. After increasing sintering temperature from 950°C to 1050°C with constant dwell time (10 min), relative density remains same (94 %), and average grain size increases. The relative density of conventionally sintered SnO_2 is same (63 %), although sintering temperature increases from 1200°C to 1400°C under constant pressure, heating rate and dwell time. Commercial target has the same relative density as conventionally sintered SnO_2.

XRD patterns of sintered ceramics are given in Fig. 3. According to the obtained results, all SPSed ceramics is composed of SnO_2 (Cassiterite; JCPDS #41-1445) as a monolithic crystalline phase except

the SPS5-SnO_2 sintered at 1050ºC that contains SnO_2 and elemental Tin (Sn; JCPDS #04-0673). Thus, it confirms that a reasonable amount of elemental Sn is formed at 1050ºC and solidifies during cooling.

3.2.1 Effect of sintering temperature on microstructure development

SnO_2 (s) ⇔ SnO (g) + ½ O_2 (g) (1)

SnO_2 (s) ⇔ Sn (l) + O_2 (g) (2)

As stated before, the relative density remains the same even though the sintering temperature is raised from 950ºC to 1050ºC, and only SPS5-SnO_2 contains elemental Tin (Sn; JCPDS # 04-0673) as a secondary phase. Rietveld analysis pattern obtained from powder diffraction data of SPS5-SnO_2 is given in Fig. 4. According to phase determination carried out by the Rietveld method, elemental Tin content in SPS5-SnO_2 is ~ 3 wt. %. There are two possible chemical reactions for the decomposition of SnO_2 which are given in (1) and (2). ΔG-Temperature diagrams for the decomposition reactions, obtained using FactSage thermochemical software (7.3 version), are illustrated in Fig. 5. Considering the vacuuming status of the SPS chamber, the atmospheric pressure value set $1x10^{-5}$ bar during calculations. ΔG values of decomposition reactions are negative above 1200ºC and 1650ºC under vacuum indicating that SnO_2 decomposition can spontaneously proceed above these temperatures in theoretically. The presence of Sn in SPS5-SnO_2, according to XRD analysis results, indicates that the external pressure (30 MPa) and the external electric field applied during the SPS process can decrease the total free energy of reaction (2). It should be considered that the external electric field increases ion migration (chemical potential) [26]. Hence, the decomposition reaction was thermodynamically favorable even at 1050ºC in comparison to 1650ºC, which is expected to occur without any electric field effect. As a result, solid SnO_2 was able to decompose into Sn (l) and O_2 (g). Following to thermal process, the solidified Sn in the structure could be detected by XRD as a minor crystalline phase.

SEM images (BSD mode) of SPS4-SnO_2 and SPS5-SnO_2 are given in Fig. 6. It is observed that the grain size of SPS4-SnO_2 is small (about 200–300 nm), grain morphology is nearly equiaxed, and grain size distribution is homogenous. Also, elemental Sn in trace amount is formed as a decomposition product, which could not be clearly observed by XRD. As seen in Fig. 6(a), Sn particles can be seen on the surface of SnO_2, having bright contrast, since decomposition of SnO_2 particles starts on grain boundaries. When the sintering temperature of SnO_2 is increased further up to 1050ºC, the grain growth is accelerated by means of agglomerated Sn grains distributed non-homogenously. In addition to that, higher content of decomposed elemental Sn can now be easily detected by XRD analysis, preventing achieving full densification due to condensation-evaporation mechanism. Delorme et al. [23] showed similar decomposition behavior of undoped SnO_2 at 1050ºC for 5 min under 37.5 MPa during SPS.

The temperature and displacement (relative piston travel) curves obtained through spark plasma sintering of SPS4-SnO_2 and SPS5-SnO_2 are demonstrated in Fig. 8. All temperature curves show one step-heating schedule. The displacement curves obtained by the piston motion demonstrate the compaction of the samples during the heating cycle as indicated by the z-axis increment. The displacement values obtained by schedule data, from the beginning of the heating stage at room temperature untill the end of the heating cycle, are 1.79 mm and 2.02 mm for SPS4-SnO_2, and SPS5-SnO_2, respectively. For these specimens, compaction occurs at an early stage due to applied pressure, expansion is observed above 400ºC because of the increase of temperature, and a high shrinkage takes place above 800ºC until the end of dwell time given at top temperature. It means that the densification starts at ~800ºC and makes a huge contribution to shrinkage (displacement). During the sintering of SPS4-SnO_2, the displacement rate (ratio of displacement to temperature) slows down at 950ºC after 3 min due to densification. However, the rising temperature or the increasing displacement does not always refer to a higher densification rate. Even though SPS5-SnO_2 is sintered at a higher temperature (1050ºC) and displacement curves indicate maximum displacement value at 2.02 mm, the relative density values of SPS4-SnO_2 and SPS5-SnO_2 are equal. In this situation, the increase of temperature leads to the formation of elemental Sn in a high amount. A rapid displacement at 1050ºC points out the ejection of Sn from the graphite mold. Considering the higher theoretical density of Sn (~7.265 g/cm^3) than that of SnO_2 (~6.9 g/cm^3) and a relatively higher content of Sn in SPS5-SnO_2, the same relative density of SPS4-SnO_2 and SPS5-SnO_2 indicates less densification of SPS5-SnO_2 in which Sn exists as a secondary phase.

As known, diffusion is the most crucial sintering mechanism. According to Arrhenius' expression,

the diffusion is temperature-dependent. Hence, the increasing sintering temperature increases the sintering rate by promoting atomic diffusion (24,27). For this reason, the effect of sintering temperature on microstructural development of SPSed ceramics has been investigated in this section. However, relative density is limited to 94% even if sintering temperature is raised from 950ºC to 1050ºC. Full densification could not be provided owing to elemental Sn as a secondary phase formed through the decomposition of SnO_2, which is consistent with the literature [21].

3.2.2 Effect of dwell time on microstructure development

The obtained results from previous SPS experiments show that 950ºC is the optimal sintering temperature because higher sintering temperature leads to the formation of secondary phase. Still, SPS4-SnO_2 contains a trace amount of elemental Sn in its microstructure. To investigate the effect of dwell time on densification, phase evolution, and microstructural development, the different dwell times (1, 3, 5, 10 min) were applied at an optimal sintering temperature (950ºC) during spark plasma sintering. As stated before, the relative density of ceramics SPSed at 950ºC increases from 82 to 94 % with the increment of dwell time from 1 min to 10 min. According to XRD patterns, they consist of only SnO_2 phase.

SEM images (BSD mode) of SPS1-SnO_2, SPS2-SnO_2, SPS3-SnO_2 and SPS4-SnO_2 are given in Fig. 9.

It is seen that the grain size of SPS1-SnO_2 and SPS2-SnO_2 is unexpectedly larger than that of both SPS3-SnO_2 and SPS4-SnO_2. The agglomerated grains in the microstructure of SPS1-SnO_2 and SPS2-SnO_2 are illustrated with red plus signs (+) in Fig. 9. Non-homogenous grain size distribution is associated with the presence of agglomerates with a size above 500 nm. However, there is no significant grain growth for SPS3-SnO_2. A further increase in dwell time up to 10 min develops a microstructure containing grains with smaller average size. Although a holding time of more than 10 min is needed to eliminate isolated pores (complete densification), the maximum dwell time is selected as 10 min to prevent further decomposition of SnO_2 and limit liquid Sn content. The grain size reduction above 5 min is associated with the starting of decomposition of SnO_2 into Sn on grain boundaries, where grain growth of SnO_2 is suppressed without affecting the densification mechanism. A slight decrease in grain size (~ 50 nm) might be attributed to decreasing volume of reduced SnO_2 into Sn at the beginning of decomposition phenomena. In addition, the particle size of starting powder is 100–200 nm, and the average grain size of SPS4-SnO_2 is found about 200–300 nm. It shows that grain growth is minimal due to different sintering mechanisms of SPS where the pulse current flows through powder particles and then the heating power is dissipating at the contact points of particles [18].

The temperature and displacement curves of SPS1-SnO_2, SPS3-SnO_2 and SPS4-SnO_2 are demonstrated in

Figure 10. The process data of SPS2-SnO_2 could not be collected because of a technical problem. The shrinkage rate remarkably increases above 800°C during the one step-heating cycles. The total displacement value is found 1.54 mm, 1.71 mm, and 1.79 mm for SPS1-SnO_2, SPS3-SnO_2 and SPS4-SnO_2, respectively. The displacement (density) non-proportionally increases with the gradual increase in dwell time. As seen in Fig. 10(b) and Fig. 10(c), the full compaction cannot be provided in 5 min because displacement ratio is high, while the displacement reaches a plateau after 5 min where the shrinkage rate is too low. On the other hand, a plateau on displacement curve refers to higher densification for SPS4-SnO_2, whereas that contains elemental Sn in trace amount. In order to produce monolithic SnO_2 ceramics with high chemical purity, 5 min is selected as the optimal sintering time for SPS.

Figure11 The schematic illustration of microstructural development of SPSed SnO_2 ceramics as a function of time and temperature

The schematic illustration of microstructural development of SPSed SnO_2 ceramics as a function of time and temperature is given in Fig. 11. To summarize the given knowledge in Sect. 3.2., both increment of dwell time from 5 to 10 min at 950°C and the increasing of sintering temperature from 950°C to 1050°C does not contribute to densification of SnO_2 (relative density remains almost the same) because of the evaporation of SnO_2 into elemental Sn followed by condensation of Sn onto SnO_2 grain boundaries that is thermodynamically favorable at 950°C under SPS conditions. The formation of Sn has been firstly seen on grain boundaries on the 10th min of sintering at 950°C. Although dwell time is increased from 5 to 10 min, a slight decrease in average grain size is observed unexpectedly, which might be attributed to

decreasing volume of reduced SnO_2 into Sn at the first moment of decomposition phenomena took place on particle surface under external pressure (30 MPa) and the external electric field. When the sintering temperature rises from 950°C to 1050°C, much more elemental Sn is formed, and liquid Sn phase is migrated through Sn grains by viscous flow under external pressure. Next, liquid Sn grains are solidified in agglomerated form (Fig. 11) under a high cooling rate (~ 600°C/min) and high vacuum ($1x10^{-5}$ bar). Also, average grain size of SnO_2 is increased expectedly with the increment of temperature from 950°C to 1050°C that refers to grain growth governed by surface diffusion, where the size of isolated pores is not decreased through grain boundary and/or lattice diffusion that keeps densification rate constant [24].

3.3 Comparison of the sintering techniques

The relative density of SnO_2 ceramics remains constant at 63 %, although the sintering temperature increases from 1200°C to 1400°C during conventional sintering. SEM images of conventionally sintered SnO_2 ceramics are given in Fig. 12. It can be seen that the increasing sintering temperature causes a remarkable enhancement in grain size. The formation of elemental Sn from SnO_2 decomposition could not be observed.

The average size of equiaxed grains is found roughly 500 nm, 1 µm, and 3 µm for CS1-SnO_2, CS2-SnO_2, and CS3-SnO_2, respectively. Without any improvement in densification, the grain growth points out the surface diffusion occurred as a dominant mass transportation mechanism [24]. Therefore, 1200°C is chosen as an optimal sintering temperature for conventional sintering to prepare the sputtering target.

There is a significant difference in relative density values of SPS3-SnO_2 and CS-SnO_2. The low relative density (63 %) indicates that the second step of sintering cannot be reached even at 1200°C for 120 min. The reason is related to not only lattice and grain boundary diffusion, but also plastic deformation and creep that took place during pressure-assisted sintering [24, 26]. A higher density is achieved under using SPS at a lower temperature in reduced time because the densification rate relative to the coarsening rate increases by pulsed current (typically a few thousand amperes) under a pulsed DC voltage and external pressure as a capillary pressure. They promote mass transport by enhancing the total interfacial energy of curvature under deformation [18, 24].

CM-SnO_2 has the same density value compared to CS-SnO_2 ceramics. It means that the commercial product was produced by a conventional (pressureless) technique.

XRD patterns given in Fig. 13 show that SPS3-SnO_2, CS1-SnO_2, and CM-SnO_2 are composed of only SnO_2 phase. Figure 14 illustrates the SEM images (SE mode) of SPS3-SnO_2, CS1-SnO_2 and CM-SnO_2. The effect of the sintering technique on the microstructure of ceramics can be easily noticed. SPSed SnO_2 has a partially dense microstructure containing fine SnO_2 grains with an average size of ~ 300 nm. Conventionally sintered SnO_2 has not a dense microstructure. Neck formation occurs without grain growth and pore isolation. SnO_2 grains in equiaxed shape have an average size of 500–600 nm. Like CS1-SnO_2, CM-SnO_2 possesses the same density and a non-dense microstructure where the sintering is

limited with neck formation. However, the grain size is larger than 3 μm, and the grains are distributed inhomogeneously. That could be caused by a coarser starting powder of CM-SnO_2 compared to CS1-SnO_2.

4 Conclusions

In the present study, SnO_2 ceramics were produced from undoped submicron SnO_2 powders using the SPS and pressureless-assisted sintering techniques by optimizing sintering conditions. The pressureless sintered SnO_2 ceramics at 1200°C-1400°C for 120 min exhibit very poor densification behavior and hence relatively low relative density (i.e., 63 % relative density) due to the dominance of non-densifying evaporation-condensation mechanism. On the other hand, monolithic SnO_2ceramics were successfully produced by SPS at 950°C for 5 min, which demonstrated 93 % relative density and homogeneous grain size distribution. These results show that the pressure assistance in SPS dominates the densifying mechanisms against to non-densifying mechanisms. In addition, they reveal the effect of process conditions and sintering technique (sintering mechanism) on densification behavior, phase evolution, and microstructural development of SnO_2 ceramics. Accordingly, SPSed SnO_2 ceramics can be used as sputtering targets to produce high quality gas sensors due to their relatively high density (93 % relative density), high chemical purity, homogeneous grain size distribution and smaller average grain size.

Declarations

Acknowledgments

This research did not receive any specific grant from funding agencies in the public, commercial, or not-for-profit sectors.

References

1. Advani GN, Jordan AG, Thin film of SnO_2 as a solid state gas sensors. *J. Electron. Mater.* 1980, 929–49
2. Pianaro SA, Bueno PR, Longo E et al (1995) A new SnO2-based varistor system. J Mater Sci Lett 14:692–694
3. Jiang L, Sun G, Zhou Z et al (2005) Size Controllable Synthesis of Monodispersed SnO2 Nanoparticles and Application in Electrocatalysts. Phys Chem B 109:8774–8778
4. Li F, Chen L, Knowles G et al (2017) Hierarchical Mesoporous SnO2 Nanosheets on Carbon Cloth: A Robust and Flexible Electrocatalyst for CO2 Reduction with High Efficiency and Selectivity. Angew Chem 56:505–509
5. Dattoli EN, Wan Q, Guo W et al (2007) Fully transparent thin-film transistor devices based on SnO2 nanowires. Nano Lett 7:2463–2469

6. Aoki A, Sasakura H (1970) Tin oxide thin film transistors. Jpn J Appl Phys 9:582
7. Moulson AJ, Herbert JM (2003) Electroceramics materials properties applications. John Wiley & Sons Inc, Chichester
8. Shaalan NM, Yamazaki T, Kikuta T (2011) Influence of morphology and structure geometry on NO2 gas-sensing characteristics of SnO2 nanostructures synthesized via a thermal evaporation method. Sens Actuators B 153:11–16
9. Khuspe GD, Sakhare RD, Navale ST et al (2013) Nanostructured SnO2 thin films for NO2 gas sensing applications. Ceram Int 39:8673–8679
10. Baik N, Sakai G, Miuro N et al (2000) Preparation of stabilized nanosized tin oxide particles by hydrothermal treatment. J AmCeram Soc 83:2983–2987
11. Aciksari C, Tuncolu IG, Suvaci E et al (2016) The Role of Cation Concentration on Particle Formation Mechanism during Hydrothermal Synthesis of Nanosized Tin Oxide (SnO2). J Aust Ceram Soc 52:60–71
12. Falk G. Sintering of Transparent Conductive Oxides: From Oxide Ceramic Powders to Advanced Optoelectronic Materials. Sintering of Ceramics - New Emerging Techniques. Lakshmanan A. Ed. London: InTech, 2012
13. Medvedovski E, Alvarez N, Yankov O et al (2008) Advanced indium-tin oxide ceramics for sputtering targets. Ceram Int 34:1173–1182
14. ï»¿Medvedovski E (2017) Tin oxide-based ceramics of high density obtained by pressureless sintering. Ceram Int 43:8396–8405
15. Hoenig CL, Searcy AW (1996) Knudsen and Langmuir Evaporation Studies of Stannic Oxide. J AmCeram Soc 49:128–134
16. ï»¿ Leite ER, Cerri JA, Longo E et al (2001) Paskocima, Sintering of ultra fine undoped SnO2 powder. J Eur Ceram Soc 21:669–675
17. Quach DV, Groza JR, Zavaliangos A et al. Fundamentals and applications of field/current assisted sinterin. Sintering of Advanced Materials - Fundamentals and Processes. Fang ZZ. Ed. Cambridge: Woodhead Publishing, 2010
18. Suarez M, Fernandez A, Menendez JL et al. Challenges and opportunities for spark plasma sintering: a key technology for a new generation of materials. Sintering Applications. Ertug B. Ed. London: IntechOpen, 2013
19. Kessel HU, Hennicke J, Schmidt J et al. "FAST" field assisted sintering technology- a new process for the production of metallic and ceramic sintering materials (Engl. Transl.). In: *Pulvermetallurgie in Wissenschaft und Praxis Band 22 - Pulvermetallurgie - Kompetenz und Perspektive*. Kolaska H. Ed. Conference Proceedings - Hagener Symposium Pulvermetallurgie, 2006
20. Yoshinaka M, Hirota K, Ito M et al (1999) Hot Isostatic Pressing of Reactive SnO2 Powder. J AmCeram Soc 82:216–218

21. Park JW, Jo W, Kim DY (2005) Enhanced densification of pure SnO2 by spark plasma sintering. Journal of Materials Science 40:3825–3827
22. Rembeza SI, Kosheleva NN, Rembeza ES et al (2014) Synthesis of Compositionally Different Multicomponent Metal–Oxide Films (SnO2)x(ZnO)1–x (x = 1–0.5). Semiconductors 48(8):1118–1122
23. Delorme F, Dujardin R, Schoenstein F et al (2019) Nanostructuring of dense SnO2 ceramics by Spark Plasma Sintering. Ceram Int 45:8313–8318
24. Kang SJL (2005) Sintering: Densification, Grain Growth and Microstructure. Elsevier Butterworth-Heinemann, Massachusetts
25. German RM (1996) Sintering theory and practice. John Wiley & Sons, New York
26. Rahaman MN (2003) Ceramic Processing and Sintering. Marcel Dekker Inc., New York
27. Mitchell BS (2004) An Introduction to Materials Engineering and Science for Chemical and Materials Engineers. John Wiley & Sons Inc., New Jersey

Figures

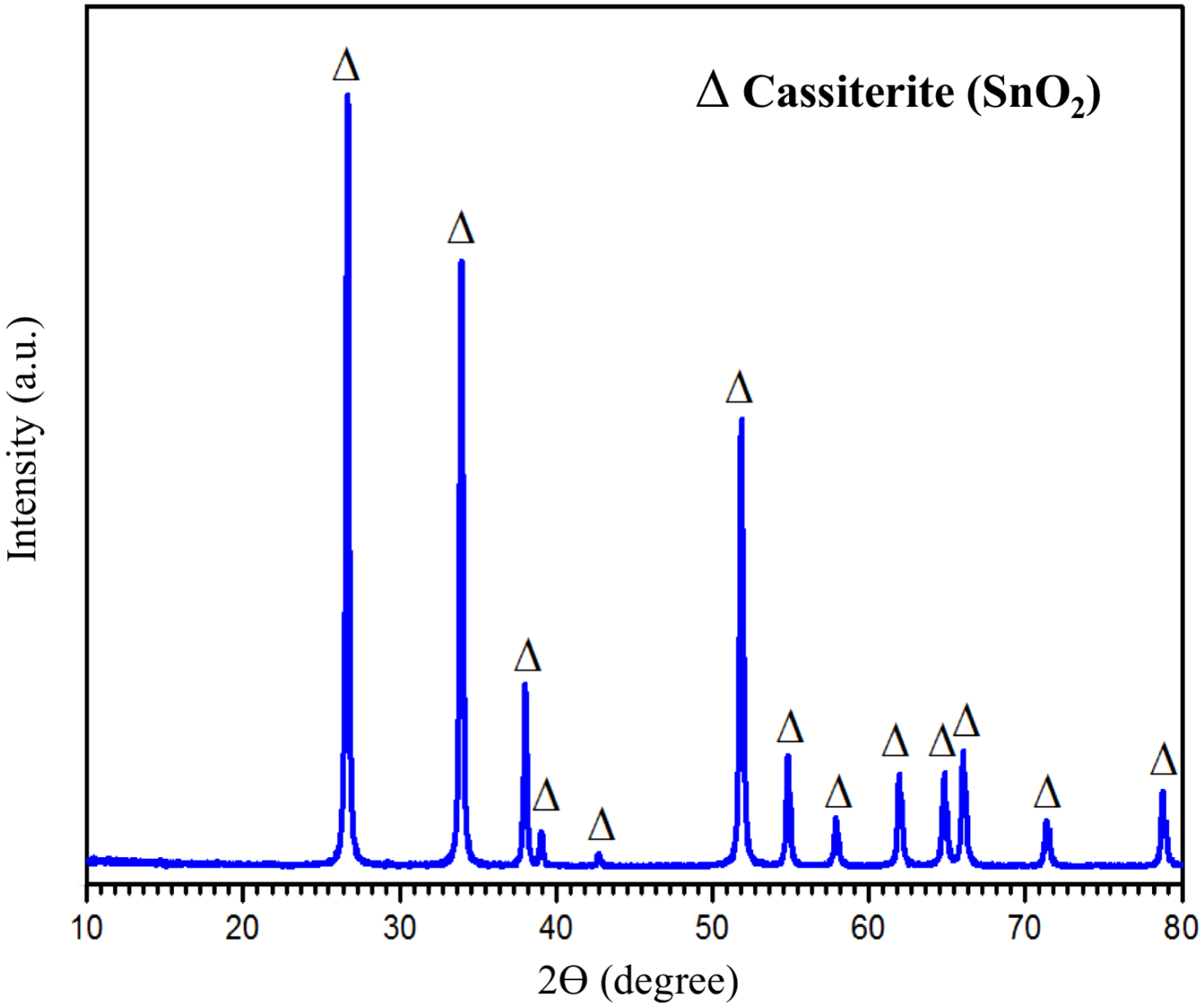

Figure 1

XRD pattern of starting powder

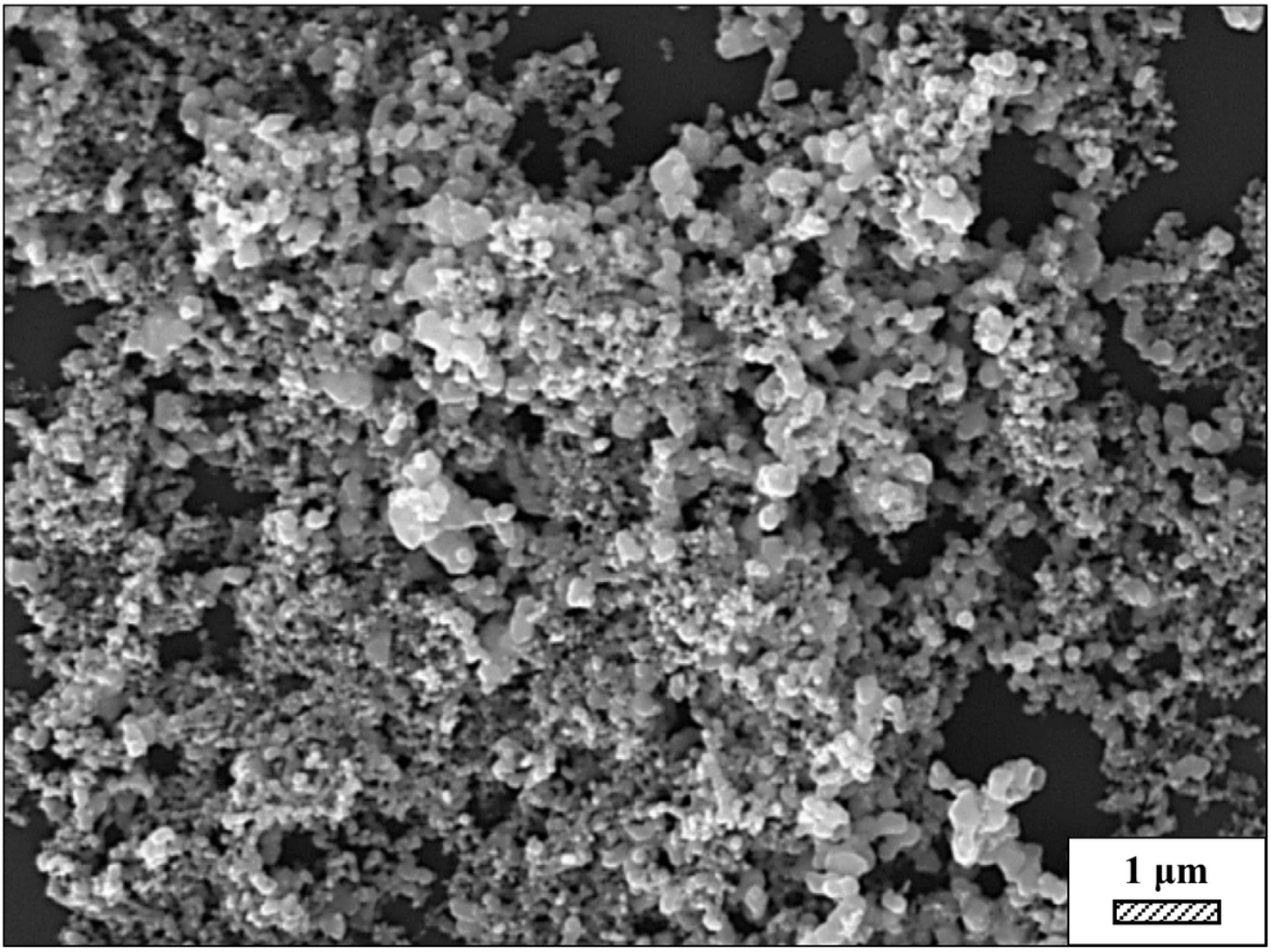

Figure 2

SEM image of starting powder

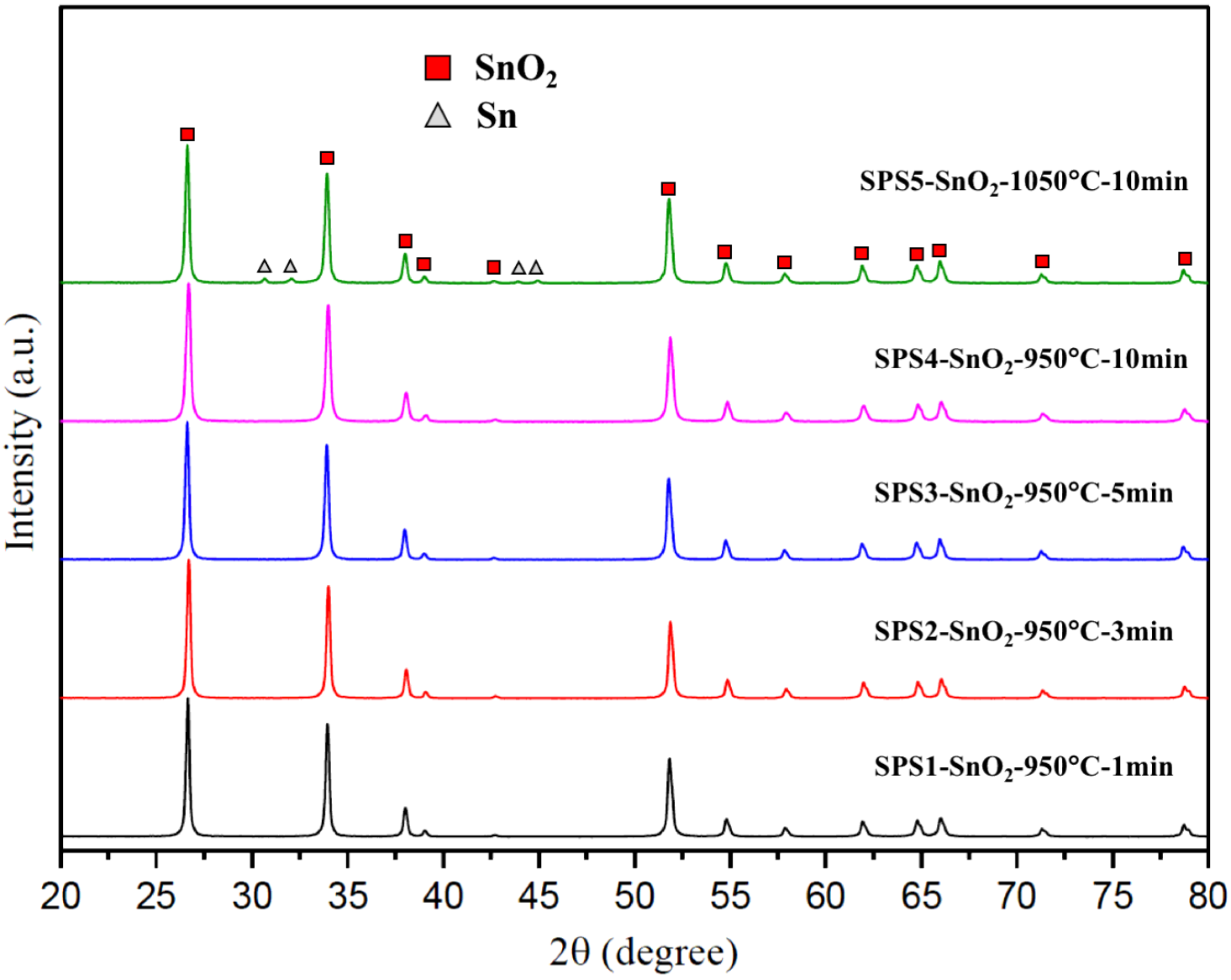

Figure 3

XRD patterns of SPS1-SnO2, SPS2-SnO2, SPS3-SnO2, SPS4-SnO2 and SPS5-SnO2

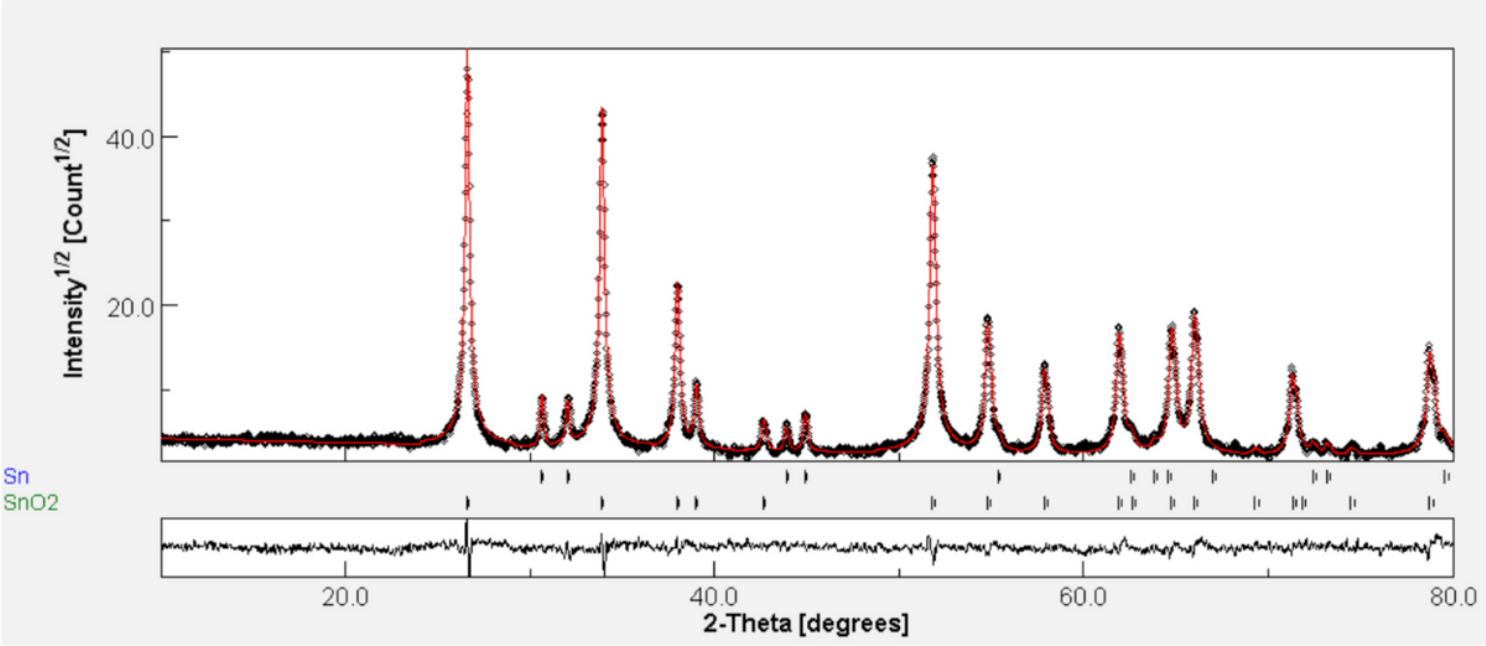

Figure 4

Rietveld analysis pattern obtained from powder diffraction data of SPS5-SnO2. The solid red lines are calculated intensities, and the black marked ones are observed intensities. The difference between the observed and calculated intensities is plotted below the profile.

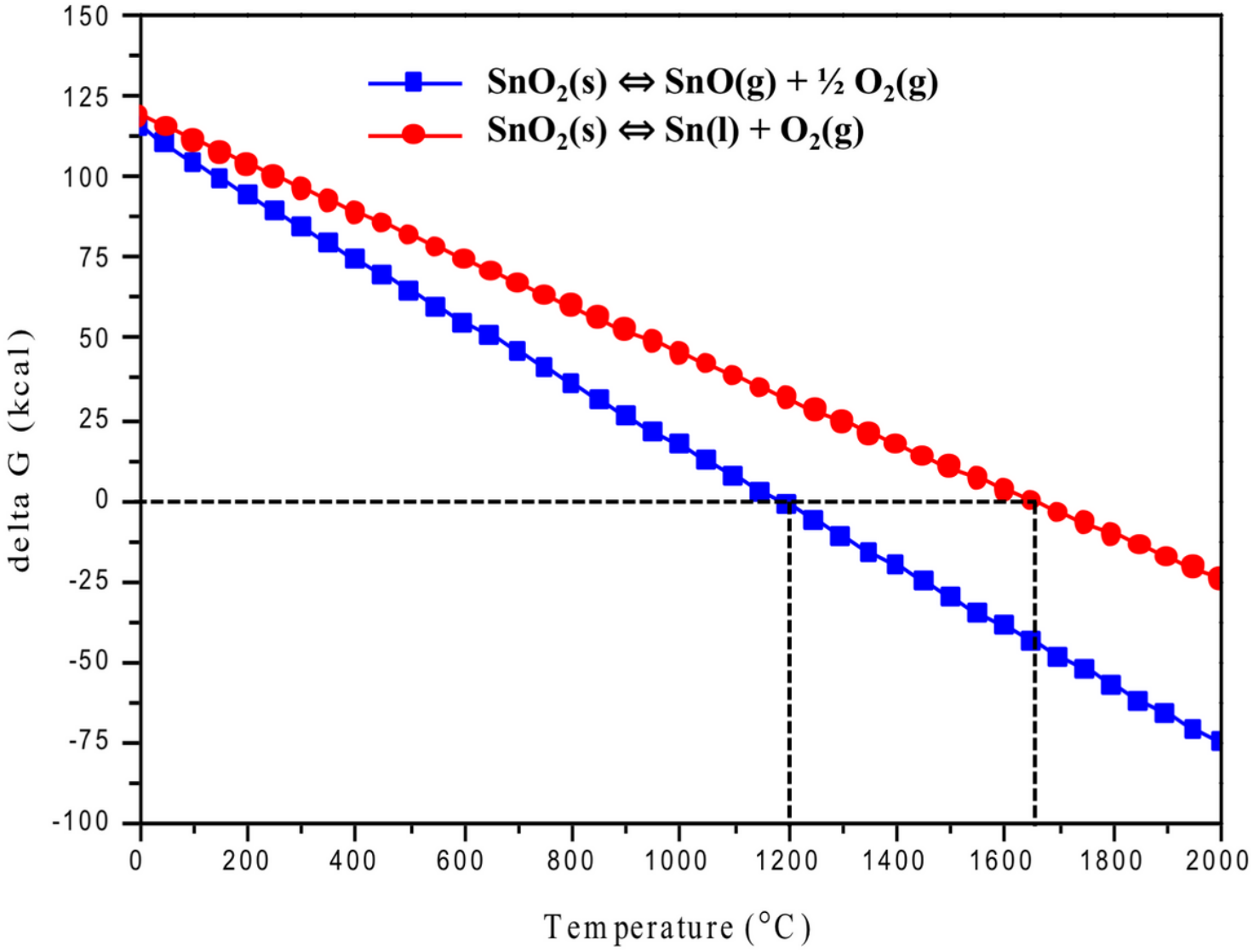

Figure 5

ΔG-Temperature diagrams for the decomposition reactions of SnO2

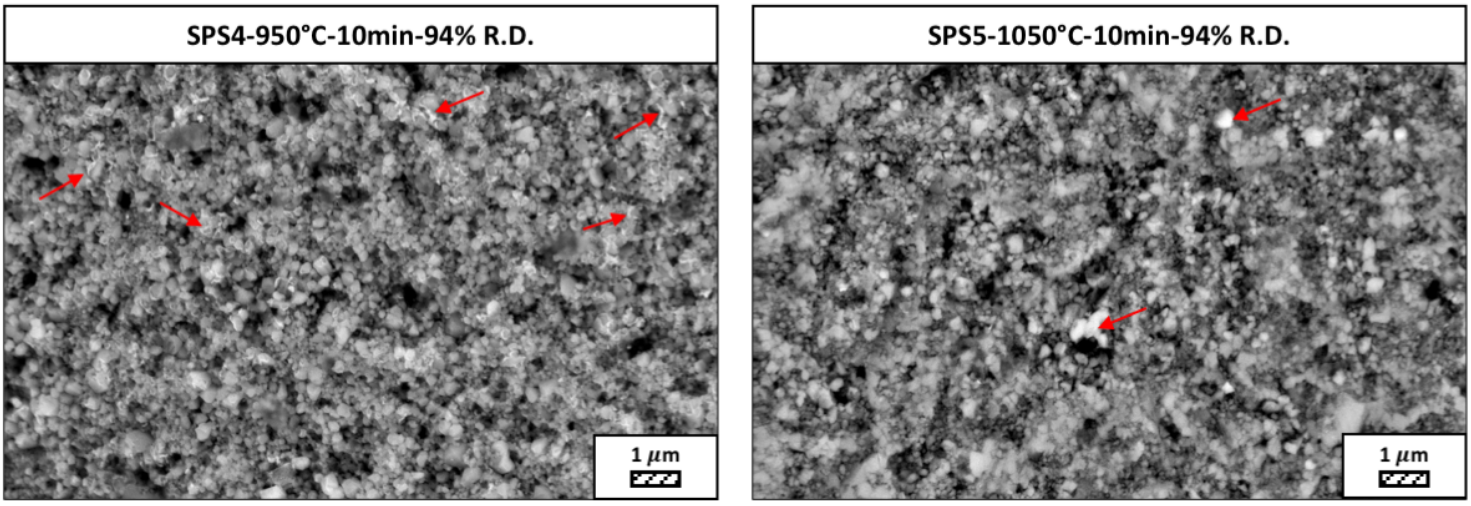

Figure 6

SEM images (BSD mode) of SPS4-SnO2 and SPS5-SnO2 at equal magnification (20.000x)

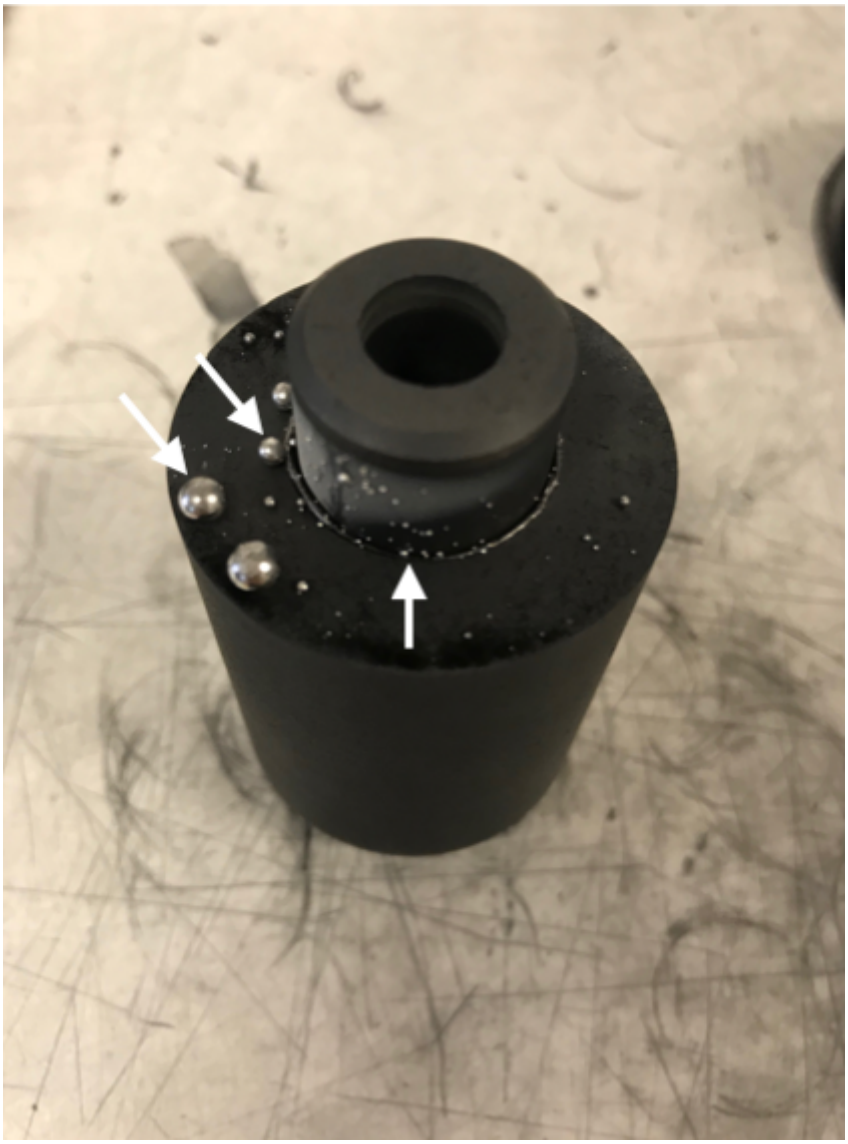

Figure 7

Image of Sn ejected from graphite mold during the sintering of SPS5-SnO2

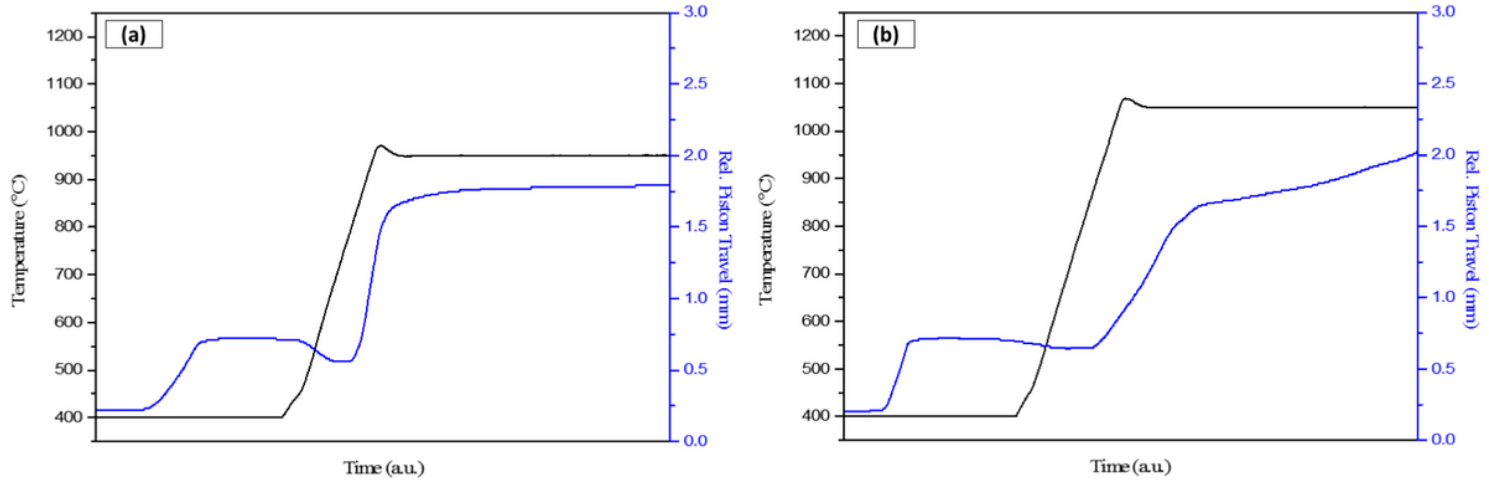

Figure 8

The temperature and displacement curves obtained through spark plasma sintering of a) SPS4-SnO2 and b) SPS5-SnO2

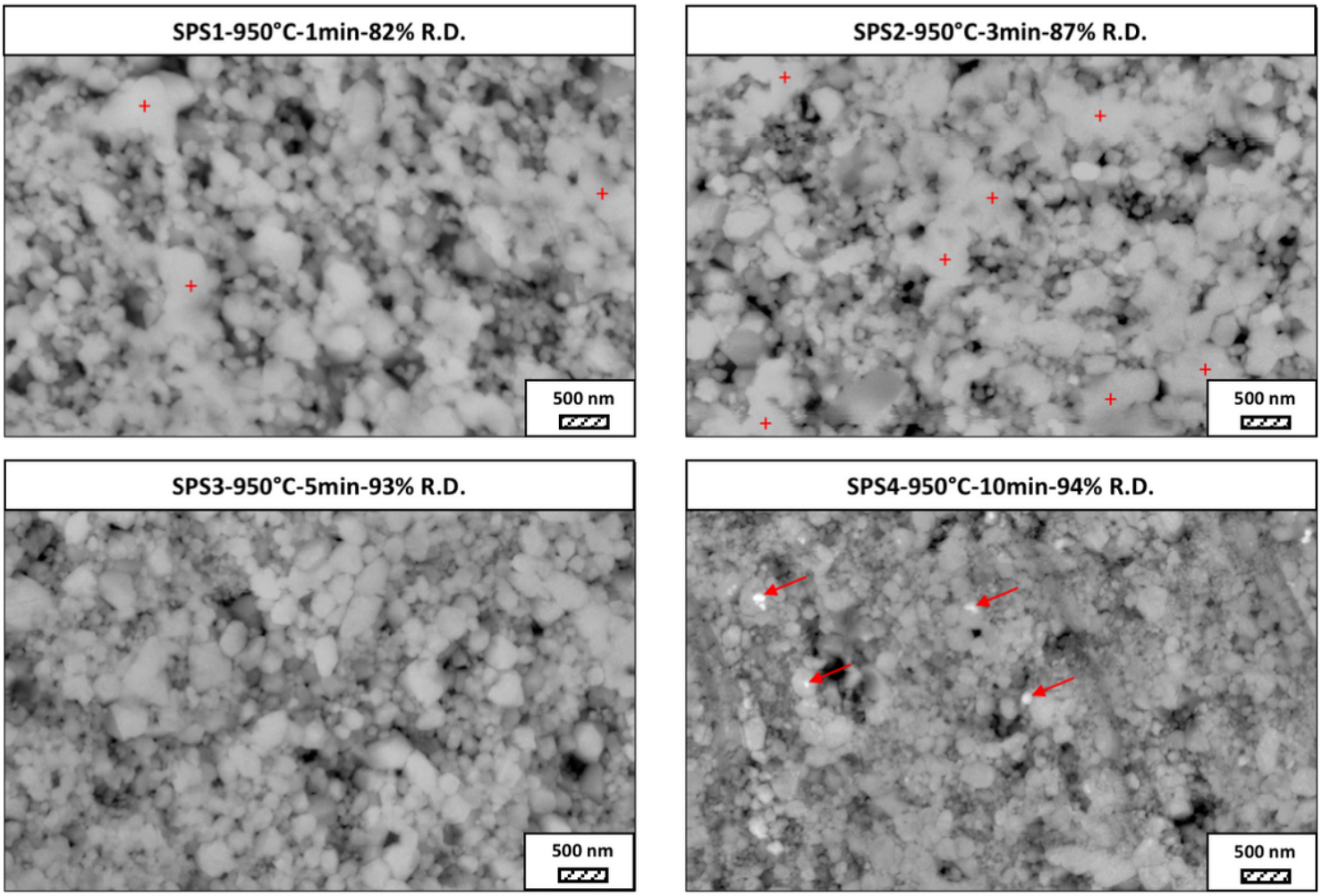

Figure 9

SEM images (BSD mode) of SPS1-SnO2, SPS2-SnO2, SPS3-SnO2 and SPS4-SnO2 at equal magnification (60.000x)

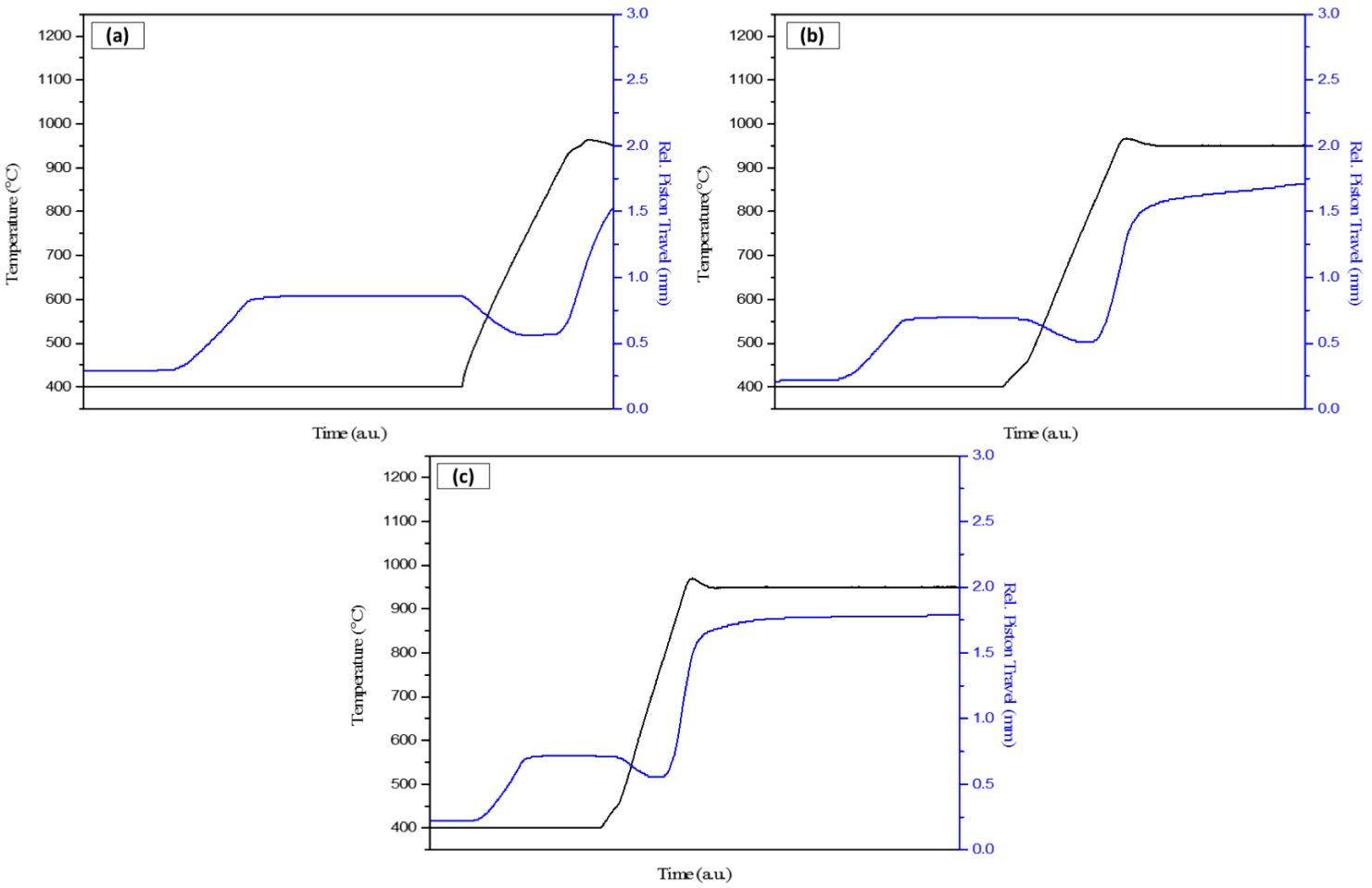

Figure 10

The temperature and displacement curves obtained through spark plasma sintering of a) SPS1-SnO2, b) SPS3-SnO2 and c) SPS4-SnO2

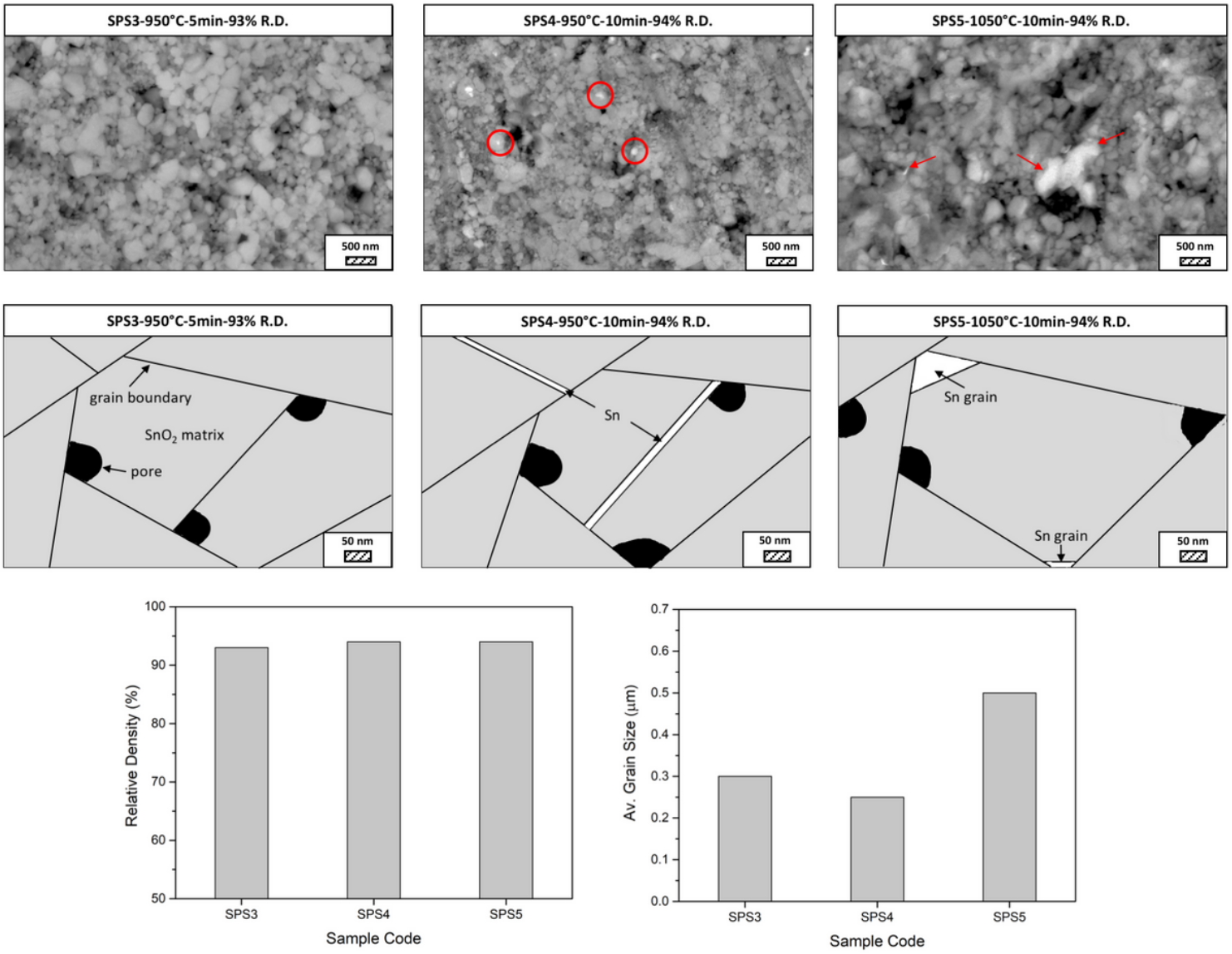

Figure 11

The schematic illustration of microstructural development of SPSed SnO2 ceramics as a function of time and temperature

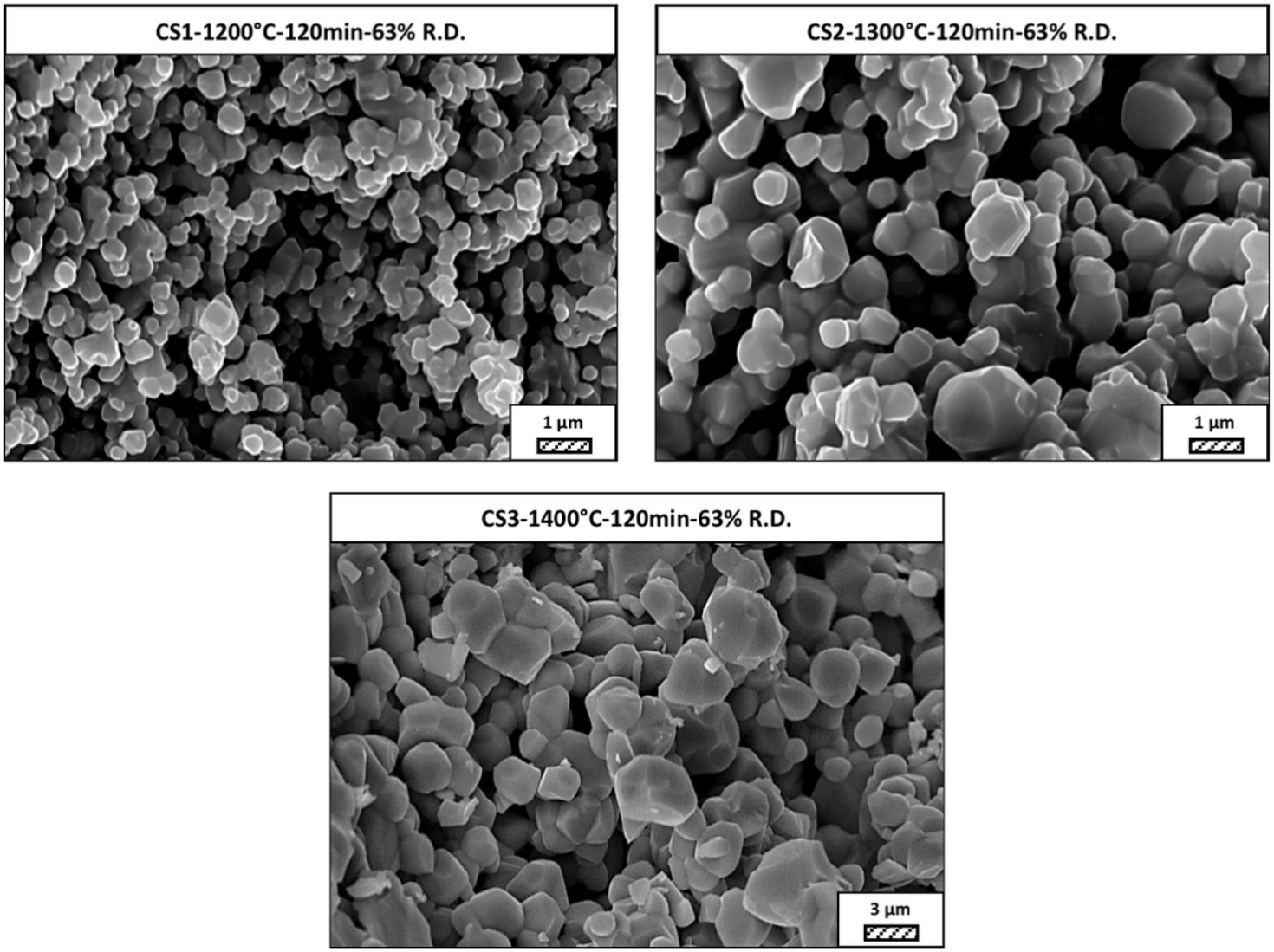

Figure 12

SEM images (SE mode) of conventionally sintered SnO2 ceramics at different temperatures

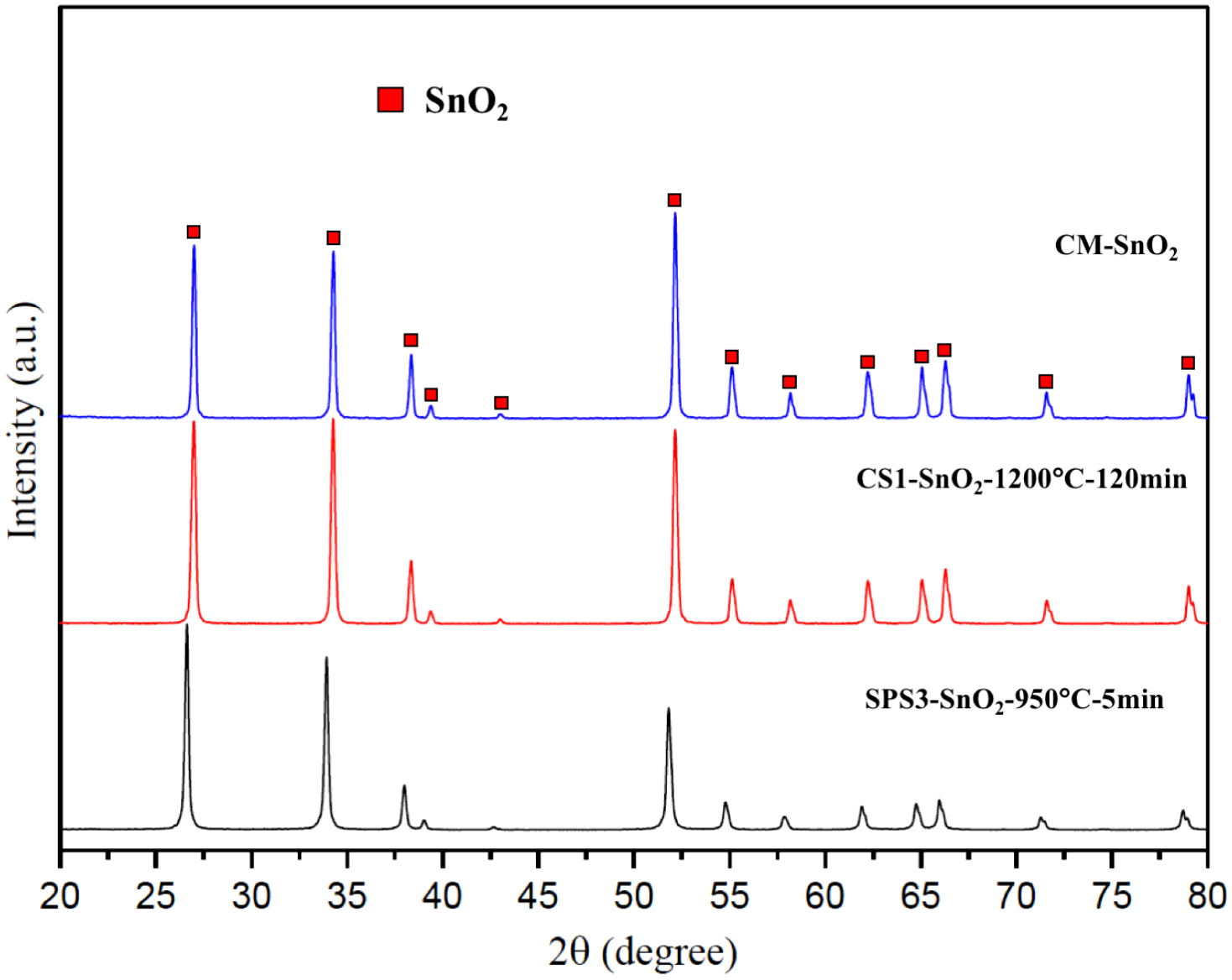

Figure 13

XRD patterns of SPS3-SnO2, CS1-SnO2 and CM-SnO2